UNCONVENTIONAL RESOURCES TECHNOLOGY CONFERENCE
FUELED BY SPE • AAPG • SEG

URTeC: 2670043

Using Fracture Stress Shadows to Drive Stage Spacing

Jonathan P. McKenna*, Michael S. Blaz, Michael H. Grealy, and Orlando J. Teran, MicroSeismic, Inc.

Abstract

Microseismic data were collected during the treatment of a four-well pad in the Williston Basin. After five months of producing hydrocarbons from the first pad, a second pad was also treated and monitored proximal to the first. Microseismic events recorded during the second pad treatment extended toward and accelerated across the first pad due to the enhanced permeability of the recently fractured first pad. We defined multiple pressure-diffusion fronts which were used to classify events associated with injected slickwater, injected gel, the offset pad, and depleted portions of the reservoir (Figure 1, for full description of procedure see McKenna et al., 2016). Stress inversions of microseismic focal mechanisms were then performed to identify spatial and temporal changes in the stress field with respect to proximity of the injection location and elapsed time after start of the injection.

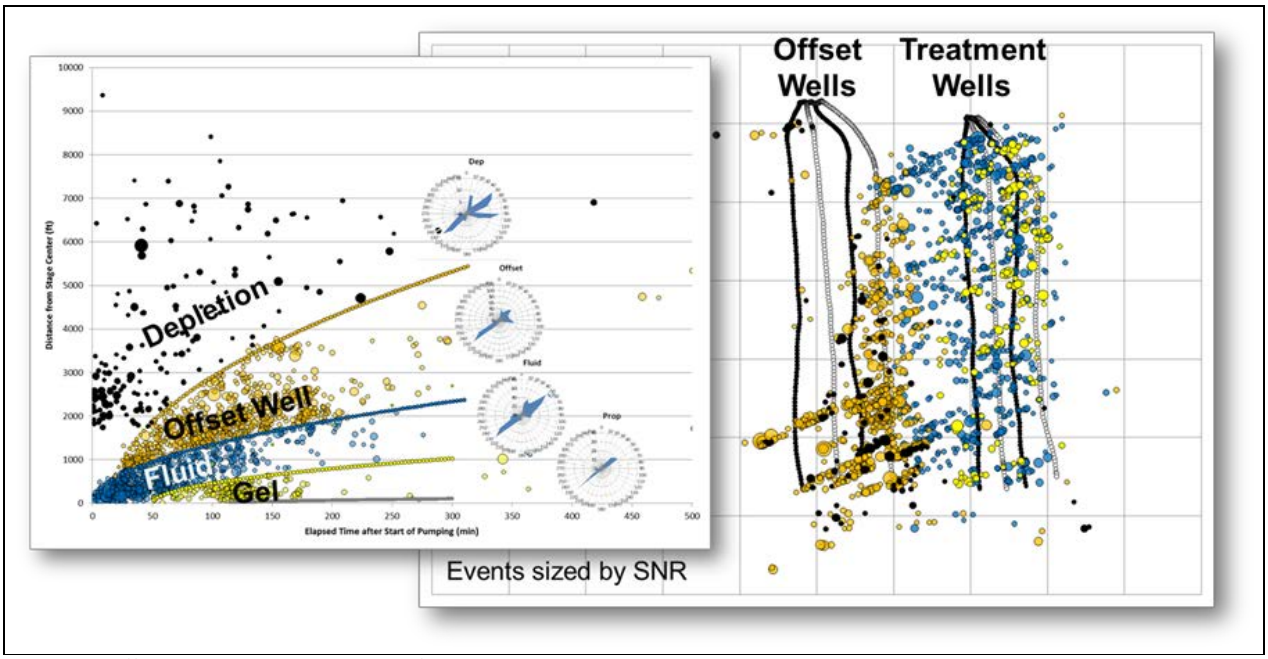

Figure 1: Offset wells drilled and produced for 5 months then treatment wells stimulated and microseismicity occurred. Events colored by classification using a method by McKenna, 2016 and sized by signal to noise ratio. Focal mechanism strike plotted on rose diagrams for each classified regime shows primary fracture set oriented ~45° with secondary sets at 20° and 90° that increases in relative magnitude with distance from stage center. Left plot axes: Elapsed time after start of pumping (min) vs. Distance from stage center (ft); Right plot axes: Easting (ft) vs. Northing (ft).

Results suggest that the initial maximum and minimum horizontal stresses (S_H and S_h respectively) are close in absolute magnitude and are subject to flipping relative to one another during the treatment and depletion of the reservoir. Stress shadowing theory suggests that the induced stress profile nearest a hydraulic fracture is anisotropic and is reversed in sign during the depleted state. Induced stress intensity is dependent on net pressure while induced stress extent is dependent upon fracture height. Because the relative magnitudes of S_H and S_h are nearly the same, depending on the relative location to another fracture and the gradient of the induced stress field, S_h can become S_H and cause the observed focal mechanisms to shift from normal dip-slip movement to oblique slip (the rake between dip-slip and strike-slip). Stress inversion results were combined with induced stress effects as a function of fracture height to identify the optimal stage spacing when S_H=S_h. The goal is to take advantage of stress shadowing effects to grow complex fractures in more of a radial fashion rather than producing long linear fractures.

Introduction

Microseismic monitoring is a proven technology for observing and mapping reservoir response to hydraulic fracture stimulations. Microseismic events are typically used to determine fracture geometry such as lateral and vertical distribution and extent. The event radiation pattern of the P-wave first arrival can reveal advanced characteristics of the fracture describing deformation at the source location. Typical focal mechanism solutions are "hand-picked" which require high signal to noise ratios and can be a laborious process (Willilams-Stroud et al., 2010) and may only be possible for a small subset of the entire microseismic population. Recent advancements have been made to automate the process allowing for a full-moment tensor solution for all microseismic events which reduces processing error and time (Kratz, 2015). The full-moment tensor can be generally decomposed into the relative percentages of isotropic, double couple and compensated linear vector dipole components (e.g. Aki and Richards, 1980) which fully describes the failure process in terms of volume change, amount of shearing, and other complexities related to deformation. The local stress field can be calculated using a set of focal mechanisms by minimizing the misfit angle between the modeled stress field and the observed focal mechanism slip vectors (Angelier, 1989) where the local stress field extent is defined by the spatial extent of the observed focal mechanisms. Consequently, in homogenous formations, slip directions with low misfit angles are preferentially aligned with the local stress field and have the highest failure tendency which requires the lowest pore pressure for failure to occur (Morris et al., 1996). Furthermore, absolute stress magnitudes can be calculated by combining relative local stress magnitudes calculated from focal mechanisms with measurements describing actual local vertical stress and minimum stress profiles assuming an Andersonian tectonic regimes (Anderson, 1951). Following Angelier (1989) the stress ratio (Φ) is calculated as follows:

$$\Phi = \frac{\sigma_2 - \sigma_3}{\sigma_1 - \sigma_3}. \quad (1)$$

Focal mechanisms describe how the rock broke during failure. There are two potential failure plane solutions for each focal mechanism. The failure plane orientation that most closely matched event trends as they occur consecutively in time was chosen as the failure plane for each focal mechanism using a method outlined by McKenna et al., 2014. In some cases, an alternative method outlined by Gephart (1985) can be used to determine the more likely nodal plane to slip once the principle stress directions and stress magnitudes have been determined.

Method and Results

Microseismic events were classified using a method outlined by McKenna et al., 2016 to separate hypocenters associated with the injected fluid of the treatment wells (Figure 1, "Fluid" and "Gel") from microseismic events that occurred on offset wells due to the depletion of the reservoir (Figure 1, "Offset well" and "Depletion"). Failure plane strike azimuths of ~45°, 20°, and 90° were observed in the data. The ~45° strike was observed in each of the classes and was primarily normal dip-slip in nature; the 20° and 90° strikes were oblique strike-slip failures that increased in relative magnitude the further from their respective stage center they occurred (Figure 1).

According to the Wallace-Bott hypothesis, shear stress resolved onto the fault plane must parallel the slip vector and consequently, slip vectors plotted on the poles of the failure plane (slip linears) point directly to the minimum principal stress, S_h. Slip linears of the dip slip events are all oriented towards an azimuth of 318° suggesting that S_h is oriented in this direction and the maximum horizontal stress, S_H is oriented at 48° (Figure 2). Since fractures typically propagate in the same direction as S_H, this stress configuration likely corresponds to the in situ stress conditions.

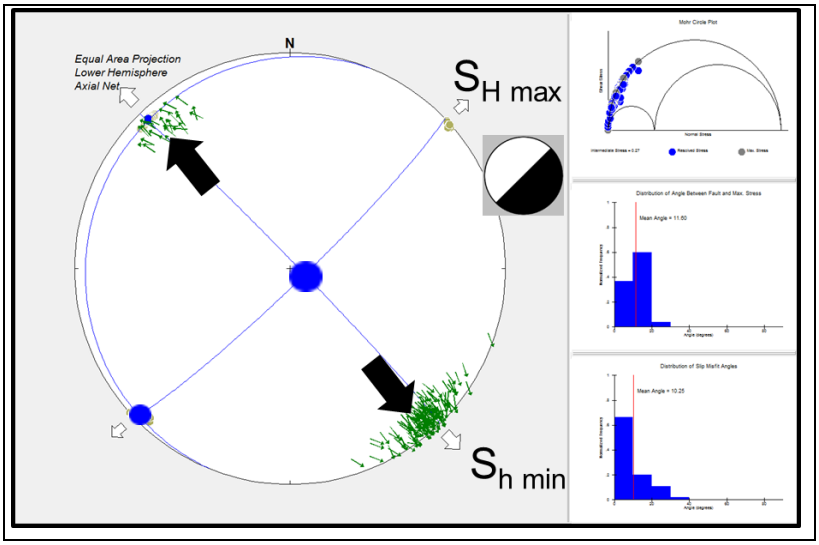

Figure 2: Left: Stress inversion results for normal dip-slip focal mechanism with signal to noise ratio>10. Events plotted as slip linears that show slip parallel direction at poles to fracture planes and blue dots are principle stress poles and sized by relative magnitude of stresses. Picture of dominant focal mechanism shown as example, black arrows show dominant slip direction. Right: Mohr circle plotted on upper right panel, distribution of angle between fault and maximum stress shown middle right panel, distribution of slip misfit angles shown on bottom right panel.

However, slip linears of the remaining non-normal are all oriented towards azimuth of 236° suggesting that S_h is oriented in this direction and the maximum horizontal stress, S_H is oriented at 56° (Figure 3). This suggests the existence of two different stress regimes where S_H is oriented ~90° from one another but in both instances ϕ<0.1 suggesting that $S_H \sim S_h$. The increase in relative magnitude of focal mechanism strikes in the 20° and 90° with increasing distance from the center of the injection stage suggests that that the in-situ stresses are altered more significantly as we move further away from the stage center and into an increasingly depleted portion of the reservoir.

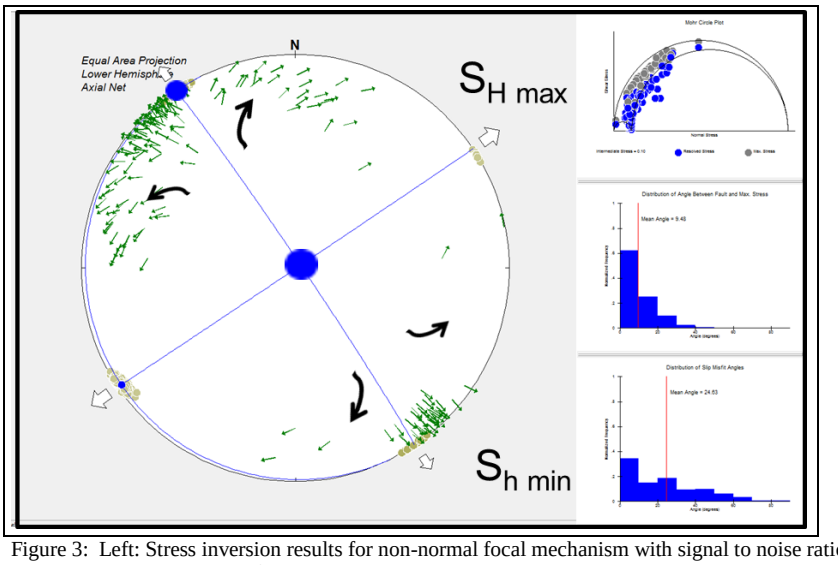

Figure 3: Left: Stress inversion results for non-normal focal mechanism with signal to noise ratio>10. Events plotted as slip linears that show slip parallel direction at poles to fracture planes and blue dots are principle stress poles and sized by relative magnitude of stresses, black arrows show dominant slip direction. Right: Mohr circle plotted on upper right panel, distribution of angle between fault and maximum stress shown middle right panel, distribution of slip misfit angles shown on bottom right panel.

Discussion and Conclusions

In order for S_h and S_H to flip in magnitude, S_h must increase in value and surpass the value of S_H. One such mechanism that can cause this phenomenon is stress shadowing. According to Figure 4, when a hydraulic fracture is created, a stress shadow is created around the induced fracture that affects smaller magnitude principal stresses more than larger stresses i.e. the effect on S_h is greater than the effect on S_H (Dohmen, 2015). Figure 4 corresponds to a total fracture height of 300 ft which was determined from the microseismic response and a net pressure of 3,500 psi which was the difference between treating pressure and minimum horizontal stress. S_H was calculated using equation 1 and measured values of S_V and S_h from Dohmen (2013) and the stress inversion derived value of ϕ=0.1 (this study).

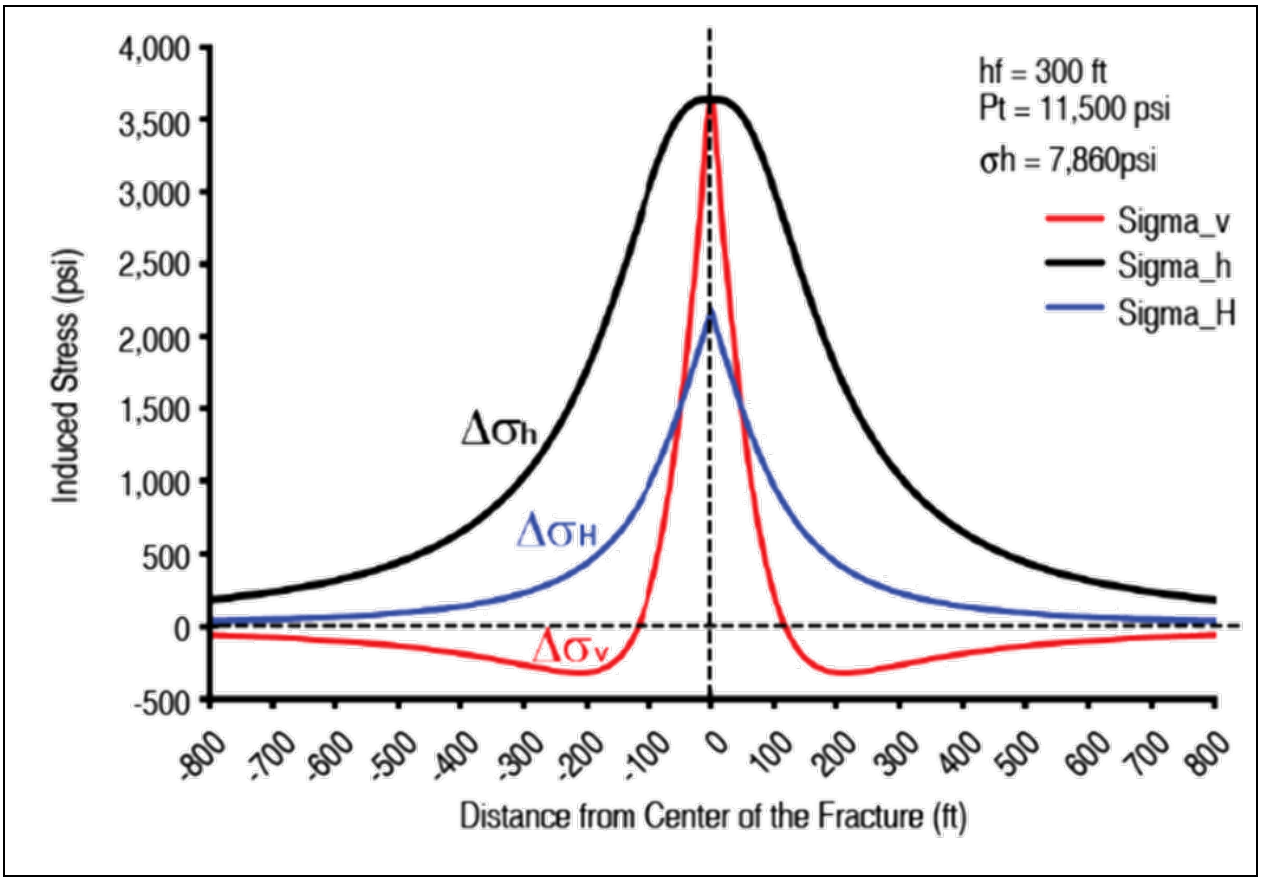

Figure 4: Stress shadow induced stress (psi) for fracture height of 300 ft for treating pressure (Pt) of 11,500 psi and minimum horizontal stress of 7,860 psi (σh) as a function of distance from center of fracture (ft) for each of the three principle stresses. Figure from Dohmen et al., 2015.

The stress-shadow profile is then combined with the in situ stresses (Figure 5) yielding a stress profile along the wellbore after the fracture was created.

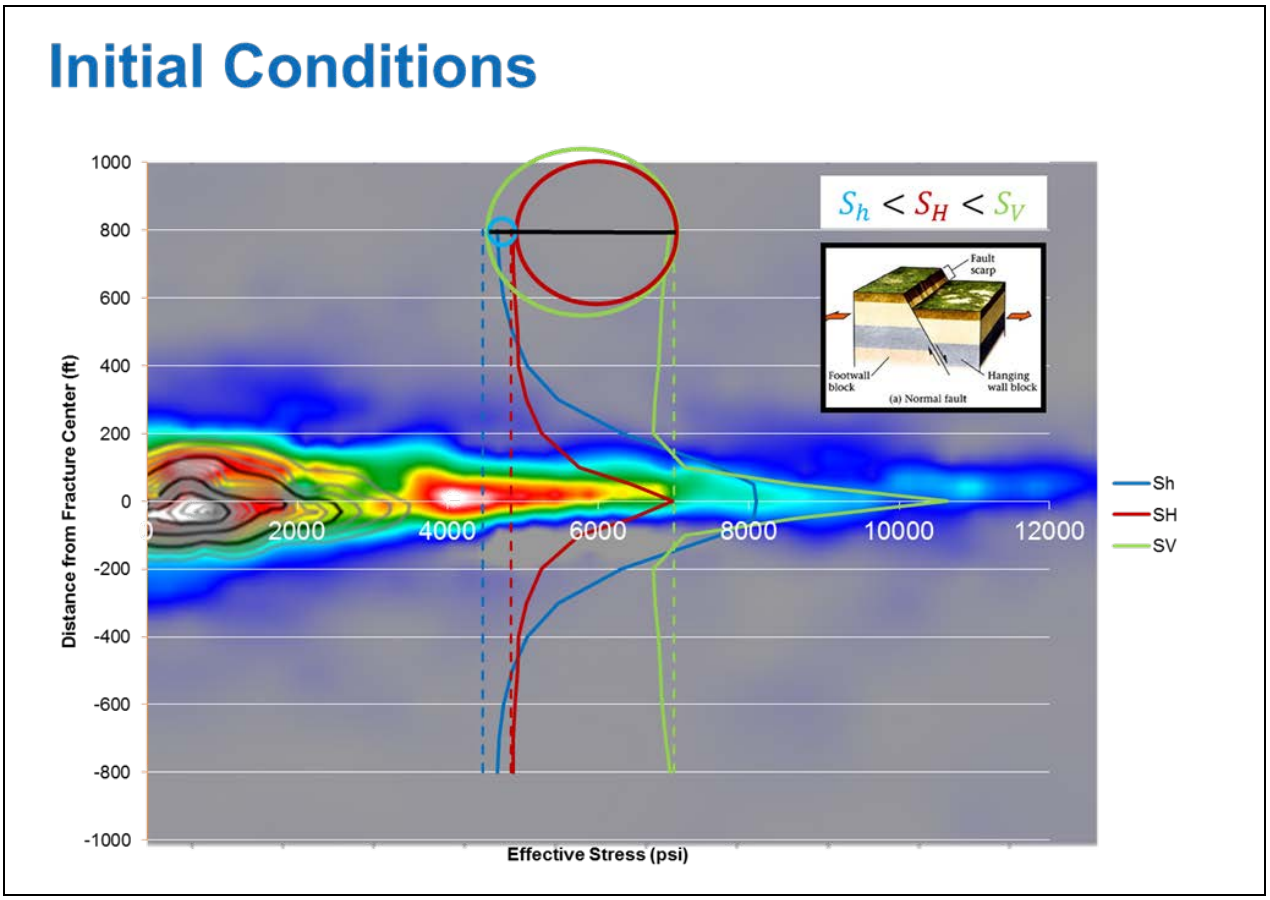

Figure 5: Stress conditions surrounding a typical hydraulic fracture (color) as a function of distance from fracture center. Mohr circle representing distributions of principle stresses along dashed lines showing stresses without stress shadow effects. Solid lines are principle stresses combined with stress shadow effects. Picture to right is schematic of observed focal mechanisms for Mohr circle.

The stress shadow begins to dissipate after pumps are shutdown, but since fractures are propped open and cannot close, the stress shadow dissipation rate is reduced and would likely still exist when the next stage begins. Figure 5 shows that the stress shadow does not extend beyond ~800 ft. where the undisturbed initial conditions exist and normal dip slip mechanisms occur. At 500 ft from the fracture, S_H=S_h and the fracture can open any horizontal direction (Figure 6). At 300 ft, the initial S_h becomes S_H and slip switches to oblique strike-slip and at 100 ft from the fracture, S_V can become the intermediate stress when strike slip faulting dominates (Figure 6).

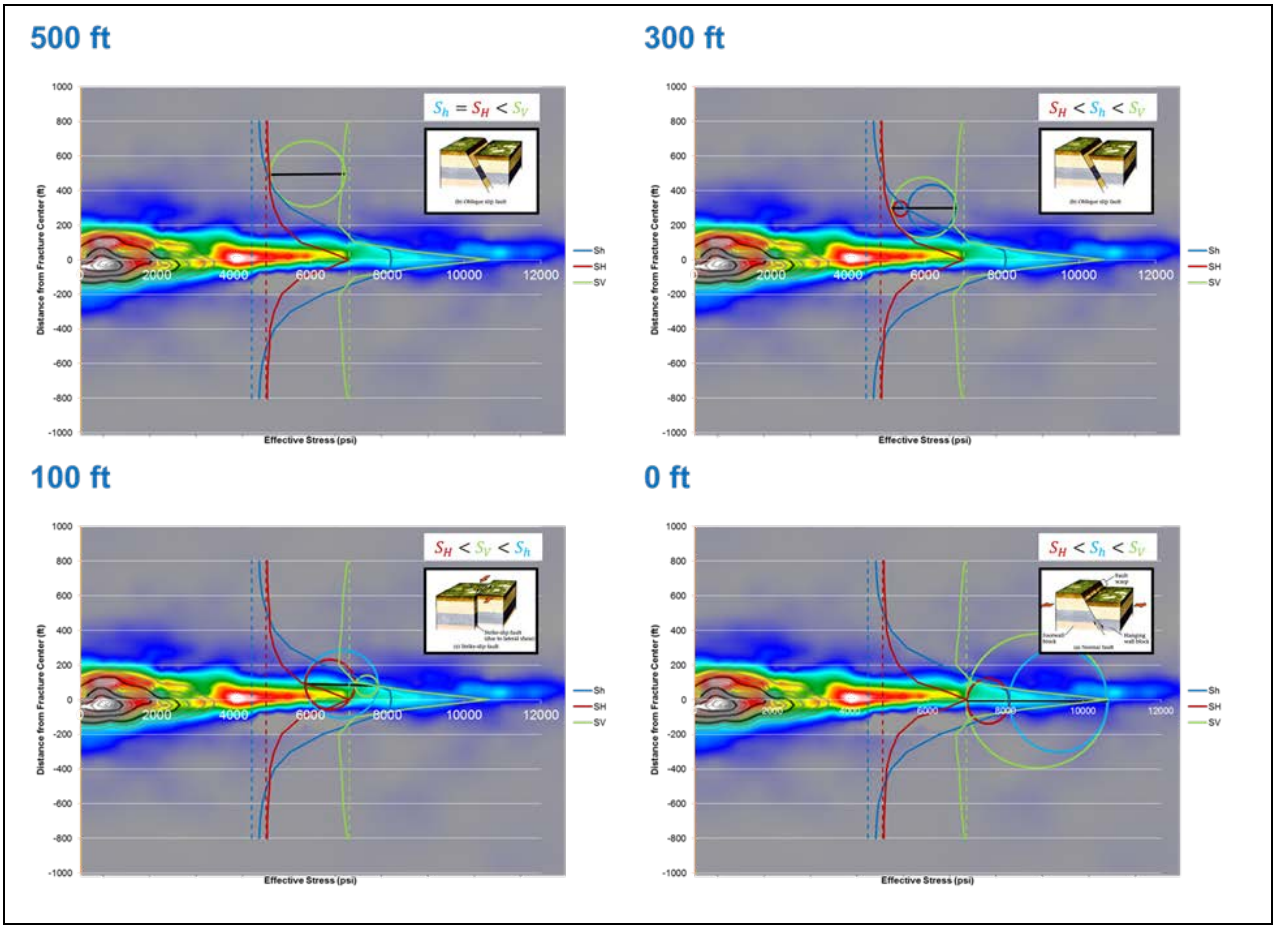

Figure 6: Stress conditions surrounding a typical hydraulic fracture (color) as a function of distance from fracture center. Mohr circle representing distributions of principle stresses along solid lines showing stresses combined with stress shadow effects. Picture to right is schematic of observed focal mechanisms for each Mohr circle.

To test the hypothesis that stress shadowing influences the change from the initial conditions (dip slip faulting) to an altered condition that favors oblique or even strike slip mechanisms, the data were aggregated by stages with the same completion types and focal mechanism rake changes were analyzed. The two completion types were single perforation cluster stages (single entry) and stages with two perforation clusters (dual entry). Only events with a signal to noise ratio > 6 were used in the analysis (Figure 7). The larger circles that indicate normal dip slip mechanisms are observed towards $+y$ values suggesting that normal dip slip mechanisms preferentially occur towards the next stage to be treated and closer to depleted wells. In other words, a stress shadow that is created around fractures from a previously treated stage results in non-normal mechanisms (smaller circles) in the direction of the previously treated stage and normal mechanisms (larger circles) in the direction moving away from the previously treated stage and the stress shadow. Similarly, normal dip slip mechanisms are located near depleted wells and shift to non-normal mechanisms away from the depleted wells indicating that the stress shadow may exist around depleted wells as well but affect the stress field oppositely, due to the negative net pressure resulting from production, as opposed to a the positive net pressure from treatment.

The stress shadow effect is also shown in Figure 8 which shows that normal dip-slip mechanisms increase in frequency as distance from the stage center increases in the direction away from the previously treated stage (+x values).

In conclusion, in the Three Forks and Bakken Formations, S_H is oriented at ~48° and ϕ=0.1 suggesting that S_H and S_h are relatively close in magnitude. Stress shadowing is a mechanism that can cause S_h and S_H to flip in magnitude

which could result in fractures opening in both directions. It may be possible to take advantage of stress shadow effects and place perforations at a sweet spot (e.g. 500 ft where S_H=S_h) so that fractures can dilate in all directions. In addition, reservoir depletion may also produce a stress shadow effect due to negative net pressure effects, but more research is required to understand this phenomenon in the depleted state.

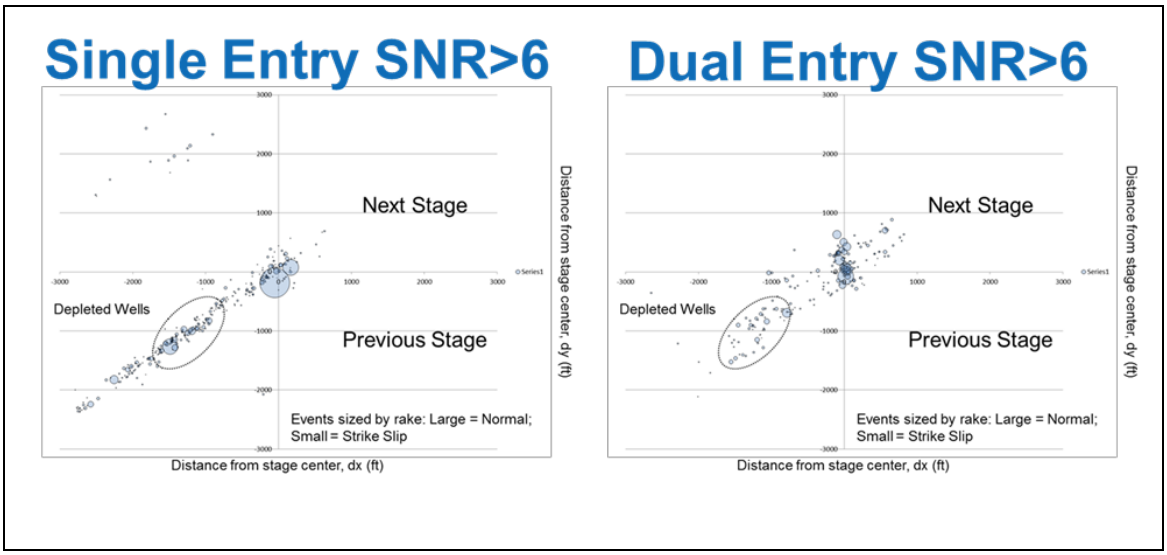

Figure 7: Events plotted as a function of distance from the stage center in dx vs dy where dy values are positive towards next stage to be treated and negative towards previous stage treated (Stages completed towards the North). Depleted well events circled and always occur along ~45° azimuth from stage treated. Events sized by rake where large circles are normal dip slip rakes and small circles are strike slip rakes. Notice that dip slip events primarily occur towards next stage away from previous stage where stress shadow exists and also near depleted wells. Top plot is aggregated for single entry stages with a single perforation injection points and bottom plot is aggregated for dual entry stages with a two perforation injection points.

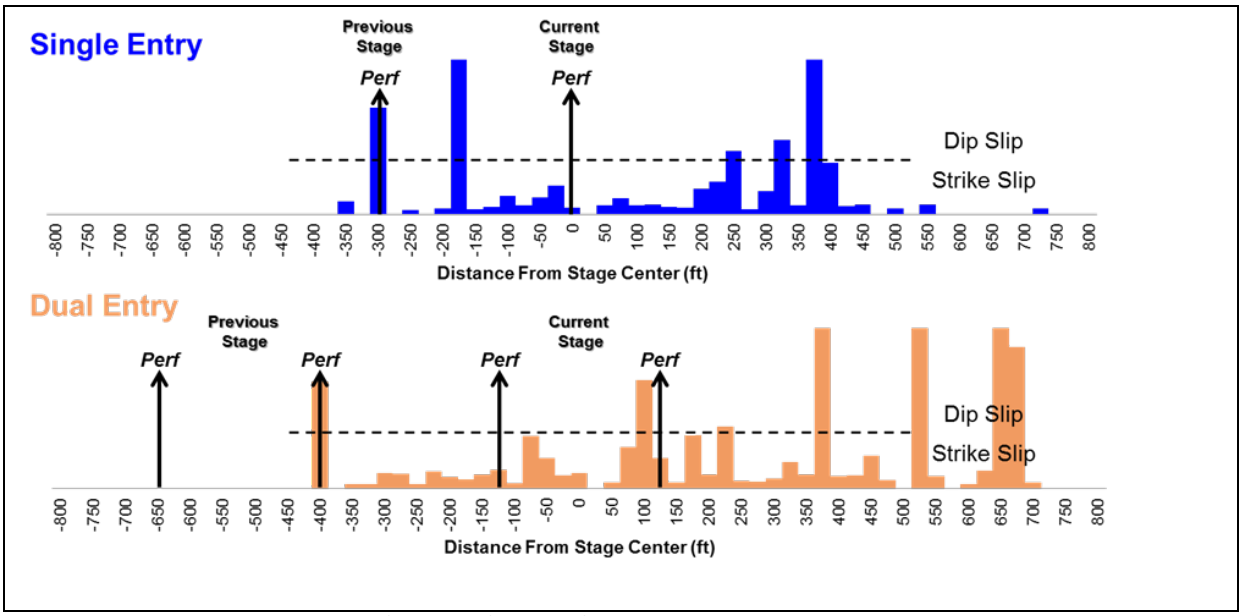

Figure 8: Histogram showing median rake for each 25 ft distance from stage center bin. Dashed line shows approximate division between normal dip slip and strike slip rakes. Top plot is aggregated for single entry stages with a single perforation injection points and bottom plot is aggregated for dual entry stages with a two perforation injection points. In general, rakes progress from strike slop to dip slip as a function of distance from the perforation on the previous stage. In addition, normal dip slip events primarily occur approximately >500 ft away from perforation from previously treated stage.

References

Aki, K., and Richards, P. G., 1980. Quantitative seismology, Theory and methods: W.H. Freeman & Co.

Anderson, E.M., 1951. The dynamics of faulting and dyke formation with application to Britian, 2nd ed., 206 pp., Oliver and Boyd, Edinburgh.

Angelier, J., 1989. From orientation to magnitudes in paleostress determinations using fault slip data, Journal of Structural Geology, 11:37-50.

Dohmen, T., Zhang, J., Li, C., Blangy, J. P., Simon, K. M.,Valleau, D. N., Ewles, J. D., Morton, S., and Checkles, S., 2013. A new surveillance method for delineation of depletion using microseismic and its application to development of unconventional reservoirs: Presented at SPE Annual Technical Conference and Exhibition, SPE 166274.

Dohmen, T., Zhang, J. J., Blangy, J.P., 2015. Stress Shadowing Effect Key to Optimizing Spacing of Multistage Fracture Stages. The American Oil and Gas Reporter.

Gephart, J. W., 1985. Principal stress directions and the ambiguity in fault plane identification from focal mechanisms. Bulletin of the Seismological Society of America, Vol. 75: 621-625.

Kratz, M., Teran, O., and Thornton, M., 2015. Use of automatic moment tensor inversion in real time microseismic imaging, DOI 10.15530/urtec-2015-2149949, URTeC Resources Technology Conference, San Antonio, TX, July 20-22, 2015.

McKenna, J. P., Toohey, N. M., 2014. Methods for determining fracture plane orientation using passive seismic signals, US 2014202688 A1.

McKenna, J.P., Grealy, M.H., Blaz, M.S. and Toohey, N.M. 2016. Using depletion microseismicity to understand producing volumes. Society of Exploration Geophysicists National Conference, Dalla, TX.

Morris, A., Ferrill, D. A., Henderson, D. B., 1996. Slip-tendency analysis and fault reactivation, Geology, 24:275-278.

Williams-Stroud, S., J. Kilpatrick, B. Cornette, L. Eisner, and M. Hall, 2010. Moving outside of the borehole: characterizing natural fractures through microseismic monitoring: First Break, v. 28/7, p.91-92.